HIGH-DEFINITION POINT CLOUD MAP-BASED 3D LiDAR-IMU CALIBRATION FOR SELF-DRIVING APPLICATIONS

S. Srinara [1, *a], Y.-T. Chiu [1, b], M.-L. Tsai [2], K.-W. Chiang [1, c]

[1] Dept. of Geomatics, National Cheng Kung University, Tainan, Taiwan - [a] surachetsrinara@gmail.com, [b] p66081106@gs.ncku.edu.tw, [c] kwchiang@geomatics.ncku.edu.tw
[2] High Definition Map Research Center, Dept. of Geomatics, National Cheng Kung University, Tainan, Taiwan - taurusbryant@geomatics.ncku.edu.tw

Commission I, WG I/7

KEY WORDS: LiDAR-IMU calibration, high-definition point cloud map, INS/GNSS integration, direct georeferencing, LiDAR scan matching, least-squares adjustment.

ABSTRACT:

The multi-sensor fusion scheme has become more and more popular these days with its great potential to estimate reliable navigation information for the modern development in automated driving system (ADS) and mobile mapping systems (MMS). Since these systems are combined with numerous navigation sensors, thus their geometric relationship should be precisely known. This study focuses on practical aspects when calibrating LiDAR-IMU mounting parameters (lever-arms and bore-sight angles) in land-based MMS. This calibration model is based on expressing the mounting parameters within the direct georeferencing equation for each epoch time and conditioning a set of INS/GNSS and LiDAR navigation solutions to lie on it. There is no need for a required information about the planar features in the calibration field as part of the unknowns. Such conditions are only benefitable in the residential area where the presence of sufficient planes in form of building is abundant. We present an approach for recovery the mounting parameters by conditioning the high-definition (HD) point cloud map-based LiDAR information and INS/GNSS navigation solutions through the least-squares solutions. The presented results and discussion mainly focus on practical examples with data from land-based MMS. Preliminary results indicate that correct calibration parameters are not only capable to improve the performance of point cloud georeferencing but also dramatically provide reliable performance evaluation of navigation estimation. Moreover, these findings show that the studied method is not only applicable in the featureless environment but also in its practicality to the self-driving applications.

1. INTRODUCTION

To obtain an accurate georeferenced LiDAR scan of point clouds and navigation evaluation in MMS and ADS, LiDAR mounting parameters (i.e., lever-arm and bore-sight angles) need to be considerably estimated. There are several LiDAR calibration approaches have been proposed and developed over the past decade. For an example, the adopted approach (Skaloud and Schaer, 2007) based on the functional model for the recovery of calibration parameters through the automated detection and extraction of the planar section of the rooftops in airborne LiDAR system (ALS). This functional model is based on conditioning the georeferenced LiDAR target points to lie on surface planes (Skaloud and Lichti, 2006). Moreover, there is an approach that also followed an above functional model but adopted into their land-based mobile laser scanning system for estimating LiDAR mounting parameters (Tsai et al., 2018). As same as previously mentioned methods, most the existing strategies still relied on the specific planes (surface normal), key feature points (e.g., edges and cylinder object points) (Lv et al., 2020; Liu and Li, 2019), and locally conducted in the preferable laboratory and indoor environment (Le Gentil et al., 2018; Liu, 2017). Considering to such the procedures, LiDAR odometry (LO) is used to perform a single or multi-feature-based registration for LiDAR pose estimates and then formulate the calibration estimation model. For initialization in LO, only an Inertial Measurement Unit (IMU)-derived information is solely used to initialize LiDAR registration. In such a situation, LO accuracy may suffer from the features used (Liu et al., 2020), quality of initial pose, and prior point cloud map. Furthermore, another calibration framework is proposed in a structured environment using a specific plane to perform LO for parameter estimation (Li et al., 2021). To this end, the drawback of these existing methods for estimating the LiDAR-IMU mounting parameters are depend on the specific feature information, reliable navigation solutions, and its limit with practicality to ADS. To obtain more applicable calibration parameters for ADS, we propose the functional model for recovery the LiDAR-IMU calibration parameters through direct georeferencing of LiDAR measurement with the INS/GNSS and HD point cloud map-based LiDAR navigation solutions.

The organization of the paper is as follows. Firstly, we introduce the LiDAR-based navigation system with including INS/GNSS integration, direct georeferencing of LiDAR measurements, and the HD point cloud map-based LiDAR scan matching. Secondly, we propose the estimation model for recovery of calibration parameters. Thirdly, we describe an experiment including the sensor configuration and environment when applying this approach to land-based mobile mapping system vehicle. Next, the experimental results are presented and discussed. After that we conclude our practical experience.

* Corresponding author: S. Srinara
Email: surachetsrinara@gmail.com

2. LIDAR-BASED NAVIGATION SYSTEM

In order to obtain an accurate navigation estimation based on LiDAR measurements, there are three remarkable steps: initial pose from INS/GNSS integration, point cloud georeferencing, and LiDAR scan matching techniques. The first step is to synchronize the time between the LiDAR data and INS/GNSS navigation solution to be the same time domain and then interpolate the navigation information. The output from this process is the initial pose of LiDAR measurements. For the second step, the direct georeferencing of LiDAR measurements is conducted regarding an initial pose obtained from previous step. The third step is to refine the LiDAR navigation solution. This process uses the HD point cloud map-based LiDAR scan matching with NDT algorithm. The output from this process is used to formulate the functional model for calibration parameter estimation. The following sections describe the INS/GNSS integration, point cloud georeferencing, and HD map-based LiDAR scan matching in details.

2.1 INS/GNSS Integration

The integration of an inertial navigation system (INS) and a global navigation satellite system (GNSS) through the Kalman filter (KF) algorithm is considerable as the most applicable approach over the stand-alone system. The INS/GNSS integration systems are categorized into two schemes; loosely coupled (LC) and tightly coupled (TC) schemes. However, applying such the TC-INS/GNSS integration system would generally provide better navigation estimation due to its complexity.

The navigation state vector (x_k) of the KF algorithm is expressed as follows:

$$x_k = \left[r, v, \psi, b_a, b_g, s_a, s_g \right]^T_{21\times1} . \quad (1)$$

where r, v, ψ = the integrated navigation solutions for position, velocity, and attitude, respectively
b_a, b_g = the biases of the accelerometers and gyroscopes, respectively
s_a, s_g = the scale factors of the accelerometers and gyroscopes, respectively.

The state prediction ($\delta x_{k|k-1}$) and measurement update (δz_k) of KF are written in the discrete-time forms as follows:

$$\delta x_{k|k-1} = \Phi_{k|k-1} \delta x_{k-1|k-1} . \quad (2)$$

$$\delta z_k = H_k \delta x_{k|k-1} . \quad (3)$$

where Φ = the state transition model
H_k = the measurement matrix

In addition to the outcome of TC-INS/GNSS integration system, the navigation solution was post-processed with the forward and backward smoothing process (Shin, 2005).

2.2 Direct Georeferencing of LiDAR Measurements

Figure 1 depicts the geometric relationship of navigation sensors on a land vehicular mobile mapping system (MMS). Using an arbitrary Cartesian mapping frame (*m*-frame), the

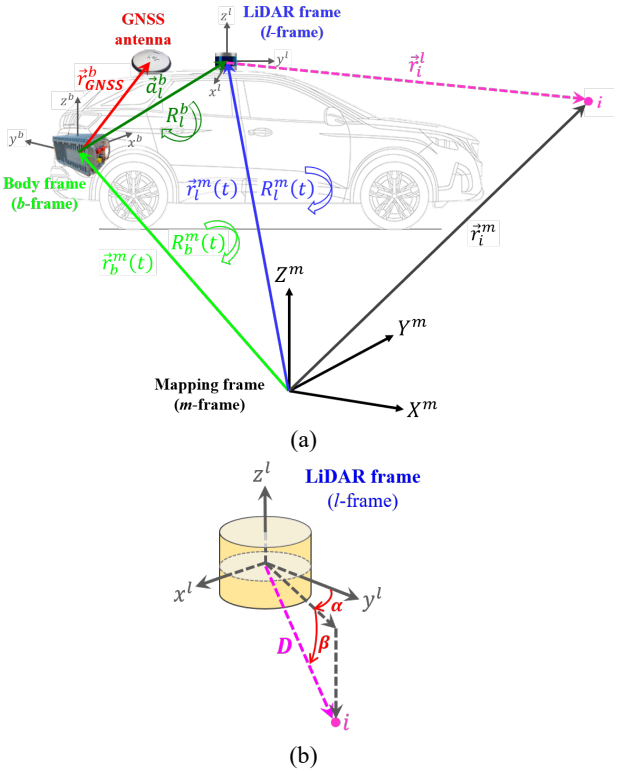

Figure 1. Direct georeferencing of LiDAR measurement: (a) geometric relationship of navigation sensor on land vehicular platform, (b) the coordinates of LiDAR measurement in the *l*-frame.

direct georeferencing of LiDAR measurements at time (t) with INS/GNSS integration system on a land vehicular platform can be expressed as follows:

$$\vec{r}_i^{\,m} = \vec{r}_b^{\,m}(t) + R_b^m(t) \cdot \left(R_l^b \cdot \vec{r}_i^{\,l} + \vec{a}_l^{\,b} \right),$$

$$\begin{bmatrix} r_{i_X}^m \\ r_{i_Y}^m \\ r_{i_Z}^m \end{bmatrix} = \begin{bmatrix} r_{b_X}^m \\ r_{b_Y}^m \\ r_{b_Z}^m \end{bmatrix}(t)$$

$$+ R_b^m(t) \cdot \left(R_l^b \cdot \begin{bmatrix} D \cdot \cos(\beta) \cdot \sin(\alpha) \\ D \cdot \cos(\beta) \cdot \cos(\alpha) \\ D \cdot \sin(\beta) \end{bmatrix} + \begin{bmatrix} a_{l_x}^b \\ a_{l_y}^b \\ a_{l_z}^b \end{bmatrix} \right). \quad (4)$$

where $\vec{r}_i^{\,m} = \left[r_{i_X}^m, r_{i_Y}^m, r_{i_Z}^m \right]^T$ = the coordinates of LiDAR measurement *i* in the *m*-frame at time *t*
$\vec{r}_b^{\,m}(t) = \left[r_{b_X}^m, r_{b_Y}^m, r_{b_Z}^m \right]^T$ = the coordinates of IMU center in the *m*-frame obtained by INS/GNSS at time *t*
$R_b^m(t)$ = the rotation matrix from the IMU in body frame (*b*) to the *m*-frame obtained by INS/GNSS at time *t*
$R_l^b = f(\theta_x, \theta_y, \theta_z)$ = the rotation matrix from the LiDAR in LiDAR frame (*l*) to the *b*-frame parameterized by the bore-sight angles θ_x, θ_y and θ_z

$\vec{r}_i^{\,l}$ = the coordinates of the LiDAR measurement *i* in the *l*-frame at time *t*

D, β, α = the LiDAR range, vertical and horizontal angles of the LiDAR measurement *i* in the *l*-frame at time *t*, respectively

$\vec{a}_l^{\,b} = \left[a_{l_x}^b, a_{l_y}^b, a_{l_z}^b\right]^T$ = the lever-arm offset between the IMU and LiDAR centers expressed in the *b*-frame.

2.3 HD Point Cloud Map-Based LiDAR Scan Matching

In order to obtain an accurate position and orientation system (POS) of LiDAR sensor, the static map-based (i.e., scan-to-map) approach is applied in this paper. As already reported in (Magnusson, 2009), the LiDAR scan matching with the normal distribution transform (NDT) provides more robust and better pose estimate than using the iterative closest point (ICP) variants.

The proposed LiDAR scan matching algorithm follows the workflow depicted in Figure 2. As mentioned earlier, the need for LiDAR-based navigation estimation with scan-to-map approach arises from the LiDAR measurements and their corresponding transformation by the integrated INS/GNSS solution. To appropriately align a LiDAR scan to a prior map and prevent NDT algorithm from trapping into local minima, it needs the reliable navigation solutions to estimate an initial pose for LiDAR registration. It proceeds through the time synchronization and interpolation process. For simplicity, the proposed LiDAR scan matching algorithm proceeds in three main steps: pre-processing and georeferencing point cloud, map extraction, and NDT pose estimate. The outcome of this process is the LiDAR pose (i.e., translation vector and rotation matrix) with respect to the *m*-frame. More details on the NDT algorithm and its extension can be found in (Biber and Straßer, 2003; Magnusson, 2009).

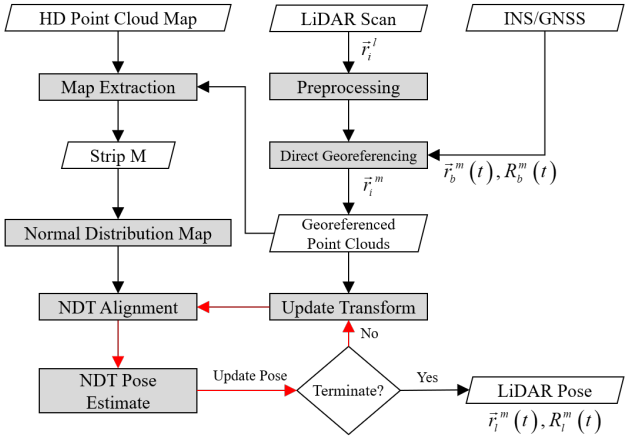

Figure 2. Workflow of proposed LiDAR scan matching algorithm.

3. ESTIMATION MODEL

3.1 Functional Model

The development of the functional model is based on conditioning the NDT-estimated LiDAR's POS and integrated INS/GNSS solution. When considering the use of a navigation grade INS and dual frequency GNSS receivers, the residual effects in TC-INS/GNSS navigation estimation should be lower than other cases in position and attitude. Regarding the better georeferencing, it is assumed that the LiDAR measurements are registered perfectly with a prior map by the NDT algorithm. As demonstrated by Figure 1, the lever-arm vector (a_l^b) and the rotation matrix (R_l^b) can be formulated herein as:

$$\vec{a}_l^{\,b} = R_m^b(t) \cdot \left(\vec{r}_l^{\,m}(t) - \vec{r}_b^{\,m}(t)\right) \cdot \tag{5}$$

$$R_l^b = R_m^b(t) \cdot R_l^m(t) \cdot \tag{6}$$

where $\vec{r}_l^{\,m}(t) = \left[r_{l_x}^m, r_{l_y}^m, r_{l_z}^m\right]^T$ = the coordinates of LiDAR center in the *m*-frame obtained by NDT algorithm at time *t*

$R_l^m(t)$ = the rotation matrix from the LiDAR in the *l*-frame to the *m*-frame obtained by NDT algorithm at time *t*.

The observation equation at time *t* expressed by the LiDAR scan matching results and INS/GNSS navigation solutions on the geometric relationship of direct georeferencing:

$$\left\langle \begin{bmatrix} \vec{r}_b^{\,m}(t) \\ R_b^m(t) \end{bmatrix}, \begin{bmatrix} \vec{r}_l^{\,m}(t) \\ R_l^m(t) \end{bmatrix}, \begin{bmatrix} \vec{a}_l^{\,b} \\ R_l^b \end{bmatrix} \right\rangle = 0 = f\left(\vec{l}, \vec{x}\right) \cdot \tag{7}$$

The observations ($\vec{l}(t)$) at time *t* is a function expressed by the position and attitude of the INS/GNSS navigation solution and LiDAR scan matching results, respectively. While the calibration parameters ($\vec{x}$) of LiDAR and IMU are represented by the lever-arm and bore-sight angles:

$$\vec{l}(t) = \left[r_{b_X}^m, r_{b_Y}^m, r_{b_Z}^m, \omega_{b_X}, \varphi_{b_Y}, \kappa_{b_Z}, r_{l_x}^m, r_{l_y}^m, r_{l_z}^m, \omega_{l_x}, \varphi_{l_y}, \kappa_{l_z}\right]^T \cdot \tag{8}$$

$$\vec{x} = \left[a_{l_x}^b, a_{l_y}^b, a_{l_z}^b, \theta_x, \theta_y, \theta_z\right]^T \cdot \tag{9}$$

The functional model used for the parameter estimation:

$$f_1 = \vec{a}_l^{\,b} - R_m^b(t) \cdot \left(\vec{r}_l^{\,m}(t) - \vec{r}_b^{\,m}(t)\right) = 0\,,$$

$$\begin{bmatrix} f_{x_1} \\ f_{y_1} \\ f_{z_1} \end{bmatrix} = \begin{bmatrix} a_{lx}^b \\ a_{ly}^b \\ a_{lz}^b \end{bmatrix} - \begin{bmatrix} c_{11} & c_{12} & c_{13} \\ c_{21} & c_{22} & c_{23} \\ c_{31} & c_{32} & c_{33} \end{bmatrix}(t) \cdot \left(\begin{bmatrix} r_{l_X}^m \\ r_{l_Y}^m \\ r_{l_Z}^m \end{bmatrix} - \begin{bmatrix} r_{b_X}^m \\ r_{b_Y}^m \\ r_{b_Z}^m \end{bmatrix} \right)(t) = 0 \tag{10}$$

$$f_2 = R_l^b - R_m^b(t) \cdot R_l^m(t) = 0\,,$$

$$\begin{bmatrix} f_{x_2} \\ f_{y_2} \\ f_{z_2} \end{bmatrix} = \begin{bmatrix} b_{11} & b_{12} & b_{13} \\ b_{21} & b_{22} & b_{23} \\ b_{31} & b_{32} & b_{33} \end{bmatrix} - \begin{bmatrix} c_{11} & c_{12} & c_{13} \\ c_{21} & c_{22} & c_{23} \\ c_{31} & c_{32} & c_{33} \end{bmatrix}(t) \cdot \begin{bmatrix} d_{11} & d_{12} & d_{13} \\ d_{21} & d_{22} & d_{23} \\ d_{31} & d_{32} & d_{33} \end{bmatrix}(t) = 0 \quad . (11)$$

where b_{ij} = the element in row *i* and column *j* of the rotation matrix from the LiDAR in *l*-frame to the *b*-frame parameterized by the bore-sight angles θ_x, θ_y and θ_z

c_{ij} = the element in row *i* and column *j* of the rotation matrix from the *m*-frame to the *b*-frame parameterized by the angles $\omega_{b_X}, \varphi_{b_Y}$ and κ_{b_Z}

d_{ij} = the element in row *i* and column *j* of the rotation matrix from the LiDAR in the *l*-frame to the *m*-frame parameterized by the angles $\omega_{l_x}, \varphi_{l_y}$ and κ_{l_z} .

3.2 Least Squares Solution

Since the functional model are non-linear, the solution is derived using the traditional method of non-linear least-squares adjustment. The linearized system of equations takes the form:

$$V_{6m,1} = B_{6m,u} \Delta x_{u,1} + F_{6m,1}. \quad (12)$$

where V = the residual vector
B = the design matrix of partial derivatives of the function (F) with respect to the calibration parameters
Δx = the vector of corrections to the appropriate calibration parameter values
F = the functional used for the calibration parameter estimation as derived in previous subsection
m, u = the number of the epoch time *t* and unknowns, respectively.

Following standard procedures, the final form of the normal equations used herein are:

$$\begin{aligned} &\left(B_k^T B_k\right) \cdot \Delta x_k + \left(B_k^T F_k\right) = 0, \\ &N_k \cdot \Delta x_k + U_k = 0, \\ &\Delta x_k = -N_k^{-1} \cdot U_k. \end{aligned} \quad (13)$$

Once the normal equations are formed, the corrections of calibration parameters are computed from an above equation. The parameter estimates are then improved iteratively. To start the iteration solution, the approximate calibration parameters can be set to the on-site measures and zero for the lever-arm and bore-sight angles, respectively. The principal advantage of proposed method are its computational efficiency, reliability, and practicality particularly during the alignment procedures with MMS or automated driving systems.

4. EXPERIMENT

4.1 Configuration Description

A land vehicle-based mobile mapping system is adopted in our case for calibration parameter estimates. As shown in Figure 3, the experimental platform used in this study includes a navigation grade-IMU (iNAV-RQH), GNSS receiver and antenna (PwrPak7), and LiDAR (Velodyne VLP-16). Considering the calibration parameters, only a LiDAR mounted on the horizontal plane is investigated in our study.

As mentioned earlier, the navigation solution was post-processed using the TC scheme with forward and backward smoothing process through the commercial INS/GNSS software (Inertial Explorer, IE). Table 1 and Table 2 show the specification and performance characteristics of iNAV-RQH IMU and LiDAR, respectively.

Figure 3. Experimental platform with navigation sensor configuration.

	Accelerometer	Gyroscope
Bias Instability	$<15\mu g$	$<0.002^\circ / hr$
Random Walk Noise	$8\mu g / \sqrt{Hz}$	$0.0018^\circ / \sqrt{hr}$

Table 1. Specification of iNAV-RQH IMU.

	VLP-16
Max. Measurement Range	100 m
Accuracy	± 3 cm
Field of View:	
- Vertical	30°(+15° to −15°)
- Horizontal	360°
Angular Resolution:	
- Vertical	2°
- Horizontal	0.1° to 0.4°

Table 2. Performance characteristics of Velodyne LiDAR.

4.2 Environmental Description

Regarding the calibration field, we only make use of a single test field depicted in Figure 4. As will become apparent, the calibration field is essentially the flat terrain of the road with regular trees, lighting poles, and some buildings. The principal advantage of this calibration field is not only its practicality but also demonstration the effect of road geometry and components

on the quality of the calibrated parameters when applying the proposed method.

In addition to the GNSS conditions, they were almost optimal for this calibration field (indicated by the green-dashed circle in Figure 4) with favourable satellite geometry and satellite observation number. As a result, GNSS position and velocity are well observable and estimable. These facts, together with the navigation grade-IMU, contributed to the good estimation of the INS/GNSS solutions.

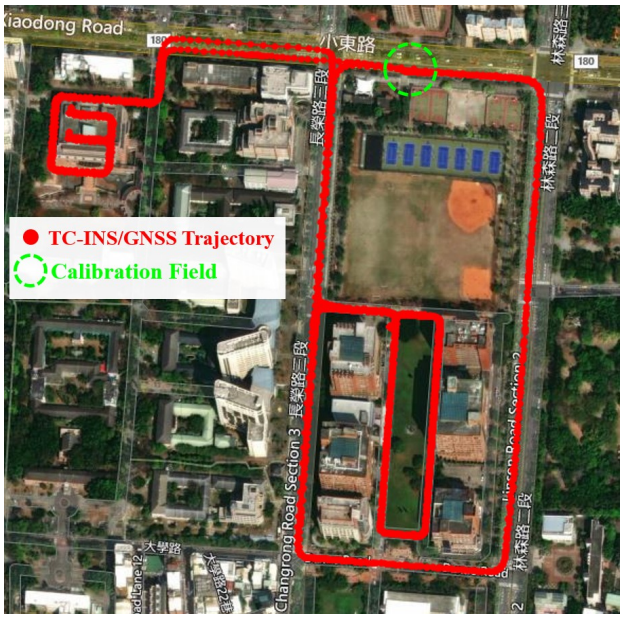

(a)

(b)

Figure 4. The experimental area: (a) bird's eye view of the INS/GNSS trajectory and calibration field, (b) real world environment of calibration field.

5. RESULTS AND DISCUSSION

To evaluate the proposed calibration method, the results are divided into three parts: calibration parameters, georeferenced point clouds, and HD map-aided LiDAR navigation estimation. For the first results, the parameters before and after calibration are presented. The second results depict the georeferenced LiDAR scan of point clouds with different calibration parameters. For the third results, the positioning differences of proposed LiDAR scan matching algorithm with different calibration parameters are analyzed. The following subsection describes the aforementioned results in details.

5.1 Calibration Parameters

As already mentioned, this study adopts the kinematic calibration model involving the INS/GNSS and NDT pose information through the direct georeferencing to construct the functional calibration model. Table 3 shows the estimated parameters before and after calibration including the lever-arm and bore-sight angles. As a result, it is clear that the calibration parameters totally differ from the initial values (i.e., before calibration) particularly a lever-arm in z-axis and all the bore-sight angles. Regarding the poor calibration parameters, this kind of error source would directly affect to the georeferenced point clouds and significantly lead to the wrong evaluation results especially in automated driving systems. In some case, the bore-sight angles can have a very small value but there should not be perfectly equal to zero. To this end, the preliminary results of proposed model seems to precisely estimate those unknowns and more practically bridge the gap of unreliable calibration parameters from manual measures.

Estimated Parameters	Before Calibration	After Calibration
$a_{l_x}^b$ (m)	0.190	0.186
$a_{l_y}^b$ (m)	0.970	0.936
$a_{l_z}^b$ (m)	1.170	1.330
θ_x (deg.)	0.000	0.889
θ_y (deg.)	0.000	-0.060
θ_z (deg.)	0.000	0.408

Table 3. Comparison of parameter estimates before and after calibration.

5.2 Georeferenced Point Clouds

In terms of LiDAR scan matching (i.e., registration), LiDAR-IMU calibration parameters take an important role for the direct georeferencing. Therefore, we can make use of the georeferenced point clouds before and after calibration to visually evaluate the calibration parameters. Figure 5 illustrates that the georeferenced LiDAR scan of point cloud (indicated by the red points) with the initial values (before calibration) has a large amount of mis-alignment particularly in the height and all the bore-sight angles compared to the HD point cloud map (indicated by the grey points). On the contrary, Figure 6 indicates that the georeferenced LiDAR scan of point clouds (indicated by the green points) with our parameters (after calibration) perfectly aligned with the HD point cloud map. It is clear that our calibration model can precisely estimate and improve the LiDAR-IMU parameters.

5.3 HD Map-Aided LiDAR Navigation Estimation

As previously described, this study makes use of the HD point cloud map-based LiDAR navigation system to estimate the LiDAR navigation state (i.e., position, velocity and attitude) and formulate the LiDAR calibration model at the same time. Table 4 shows the statistical information of positioning differences before and after calibration with the proposed LiDAR navigation algorithm at the calibration field. As a result, it is clear that the poor LiDAR mounting parameters (before calibration) lead to wrong performance evaluation in terms of positioning differences compared to TC-INS/GNSS solution. The RMS of positioning differences can reach up to 0.040, 0.019, and 0.160 meters in the east, north, and height components, respectively.

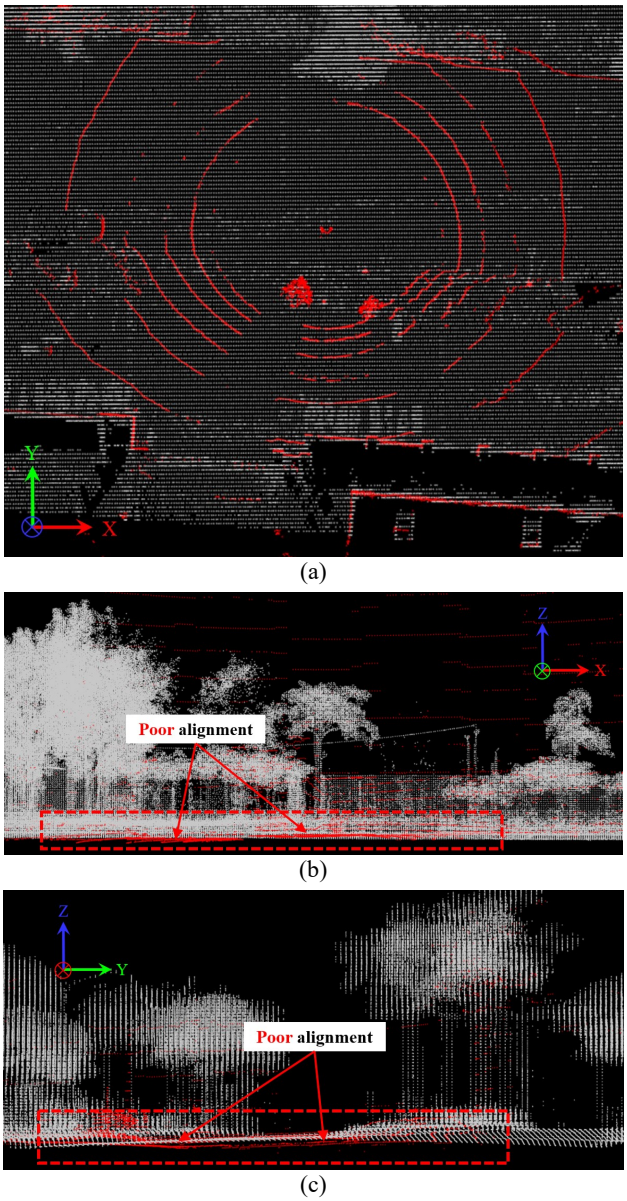

Figure 5. Georeferenced points before calibration (red points): (a) xy-plane (top-view), (b) xz-plane (side-view), and (c) yz-plane (front-view).

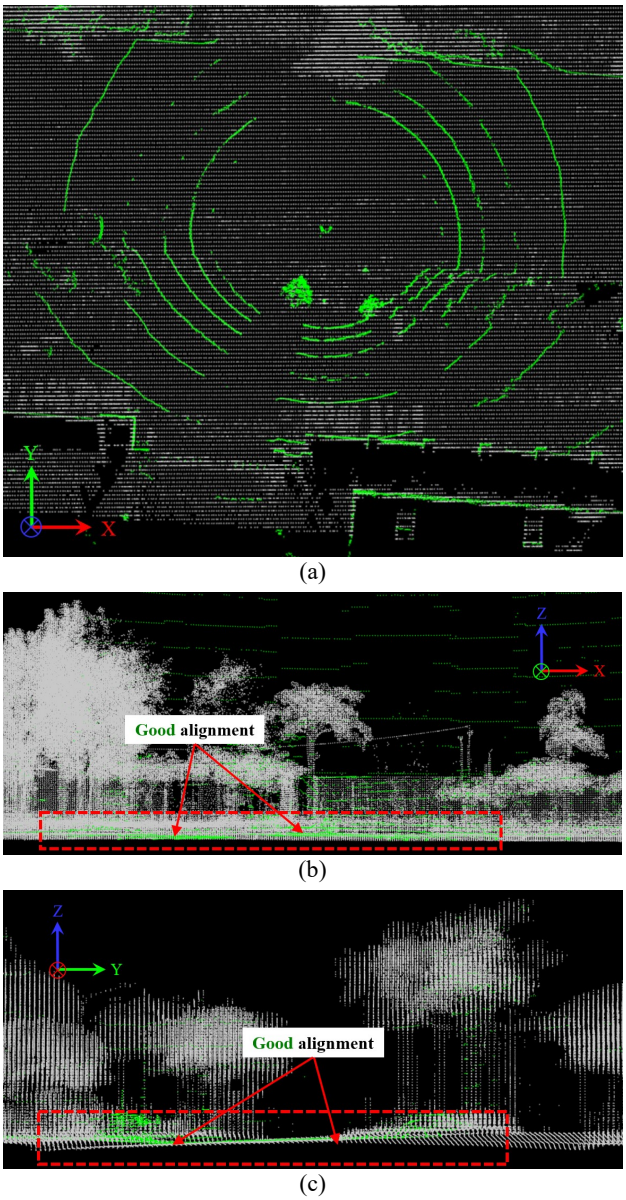

Figure 6. Georeferenced points after calibration (green points): (a) xy-plane (top-view), (b) xz-plane (side-view), and (c) yz-plane (front-view).

On the other hand, it is worth mentioning that there is a great amount of improvement with making use of our mounting parameters (after calibration). The RMS of positioning differences are only about 0.020, 0.018, and 0.056 meters in the east, north, and height components, respectively. Furthermore, the improvement is up to 50%, 5%, and 65% increases after calibration in the east, north, and height components, respectively.

Positioning Differences (m)	Before Calibration			After Calibration		
	E	N	U	E	N	U
Mean	0.036	0.011	0.150	0.011	0.011	0.049
STD	0.040	0.019	0.160	0.020	0.018	0.056
RMS	0.040	0.019	0.160	0.020	0.018	0.056
Improvement	-	-	-	50%	5%	65%

Table 4. Statistical information of positioning differences before and after calibration with the proposed LiDAR navigation algorithm.

6. CONCLUSIONS

As publicly well-known, the multi-sensor fusion scheme has a great potential to be the core navigation estimator for the modern development in automated driving or self-driving systems. To accurately obtain the best performance with low-cost LiDAR sensor to such a system, this paper proposes the calibration model to estimate the LiDAR mounting parameters using the TC-INS/GNSS and HD map-aided LiDAR navigation solutions.

As a preliminary result, accurate calibration parameters can improve the performance of point cloud georeferencing and navigation evaluation dramatically. Considering the positioning difference results in the calibration field, the experimental results show that the positioning differences has a small amount based on the parameters after calibration. Hence, the benefit of the studied method is not only applicable in the featureless environment (surface normal) but also in its practicality and

suitability to the self-driving applications since they usually make use of HD map and integrated INS/GNSS information.

ACKNOWLEDGEMENT

The author acknowledges the financial supports provided by the Ministry of Science and Technology (MOST).

REFERENCES

Biber, P., Straßer, W., 2003. The normal distributions transform: A new approach to laser scan matching. In Proceedings of Proceedings 2003 *IEEE/RSJ International Conference on Intelligent Robots and Systems*, 2743-2748

Magnusson, M., 2009. The three-dimensional normal-distributions transform: an efficient representation for registration, surface analysis, and loop detection. Ph.D. dissertation, Dept. Computer Sci., Örebro Univ.

Le Gentil, C., Vidal-Calleja, T., Huang, S., 2018. 3D Lidar-IMU Calibration Based on Upsampled Preintegrated Measurements for Motion Distortion Correction. In *IEEE International Conference on Robotics and Automation (ICRA)*, 2149-2155. doi: 10.1109/ICRA.2018.8460179.

Li, S., Wang, L., Li, J., Tian, B., Chen, L., Li, G., 2021. 3D LiDAR/IMU Calibration Based on Continuous-Time Trajectory Estimation in Structured Environments. In *IEEE Access*, vol. 9, 138803-138816. doi: 10.1109/ACCESS.2021.3114618.

Liu, W., 2017. LiDAR-IMU Time Delay Calibration Based on Iterative Closest Point and Iterated Sigma Point Kalman Filter. *Sensors*. doi.org/10.3390/s17030539

Liu, W.I., Li, Y., 2019. Error modeling and extrinsic–intrinsic calibration for LiDAR-IMU system based on cone-cylinder features. *Robotics and Autonomous Systems*, vol. 114, 124-133. doi.org/10.1016/j.robot.2019.01.010.

Liu, W., Li, Z., Malekian, R., Sotelo, M. A., Ma, Z., Li, W., 2020. A Novel Multi-Feature Based On-Site Calibration Method for LiDAR-IMU System. In *IEEE Transactions on Industrial Electronics*, vol. 67, no. 11, 9851-9861. doi: 10.1109/TIE.2019.2956368.

Lv, J., Xu, J., Hu, K., Liu, Y., Zuo, X., 2020. Targetless calibration of lidar-imu system based on continuous-time batch estimation. In *IEEE/RSJ International Conference on Intelligent Robots and Systems,* 9968-9975.

Shin, E.H, 2005. Estimation techniques for low-cost inertial navigation. Ph.D. dissertation, Dept. Geomatics Eng., Univ. Calgary, UCGE report 20219.

Skaloud, J., Lichti, D., 2006. Rigorous approach to bore-sight self-calibration in airborne laser scanning. *ISPRS Journal of Photogrammetry and Remote Sensing,* 61(1), 47-59.

Skaloud, J., Schaer, P., 2007. Towards Automated LiDAR Boresight Self-calibration. 5th International Symposium on Mobile Mapping Technology, Padova, Italy.

Tsai, G.J., Chiang, K. W.; El-Sheimy, N., 2018. Kinematic Calibration Using Low-Cost LiDAR System for Mapping and Autonomous Driving Applications. *ISPRS Int. Arch Photogramm. Remote Sens. Spatial Inf. Sci., XLII-1, 445-450*.